

AS-Bridge: A Bidirectional Generative Framework Bridging Next-Generation Astronomical Surveys

Dichang Zhang
Stony Brook University
Stony Brook, NY, USA
diczhang@cs.stonybrook.edu

Simon Birrer
Stony Brook University
Stony Brook, NY, USA
simon.birrer@stonybrook.edu

Yixuan Shao
Stony Brook University
Stony Brook, NY, USA
yixuan.shao@stonybrook.edu

Dimitris Samaras
Stony Brook University
Stony Brook, NY, USA
samaras@cs.stonybrook.edu

Abstract

The upcoming decade of observational cosmology will be shaped by large sky surveys, such as the ground-based LSST at the Vera C. Rubin Observatory and the space-based Euclid mission. While they promise an unprecedented view of the Universe across depth, resolution, and wavelength, their differences in observational modality, sky coverage, point-spread function, and scanning cadence make joint analysis beneficial, but also challenging. To facilitate joint analysis, we introduce A(stronomical)S(urvey)-Bridge, a bidirectional generative model that translates between ground- and space-based observations. AS-Bridge learns a diffusion model that employs a stochastic Brownian Bridge process between the LSST and Euclid observations. The two surveys have overlapping sky regions, where we can explicitly model the conditional probabilistic distribution between them. We show that this formulation enables new scientific capabilities beyond single-survey analysis, including faithful probabilistic predictions of missing survey observations and inter-survey detection of rare events. These results establish the feasibility of inter-survey generative modeling. AS-Bridge is therefore well-positioned to serve as a complementary component of future LSST–Euclid joint data pipelines, enhancing the scientific return once data from both surveys become available. Data and code are available at <https://github.com/ZHANG7DC/AS-Bridge>.

CCS Concepts

• **Applied computing** → **Astronomy**; • **Computing methodologies** → *Reconstruction*; *Anomaly detection*.

Keywords

Observational Cosmology, Astronomical Survey, Generative Model, Multimodal Learning

1 Introduction

In this decade, observational cosmology will be driven by major flagship surveys, such as the ground-based Legacy Survey of Space and Time (LSST) at the NSF–DOE Vera C. Rubin Observatory [19] and the space-based ESA Euclid mission [10]. Together, they provide unprecedented coverage across depth, angular resolution, wavelength, and temporal cadence, enabling major advances in topics ranging from dark energy and dark matter to asteroids and other solar system objects [4, 5, 19, 22, 31, 33].

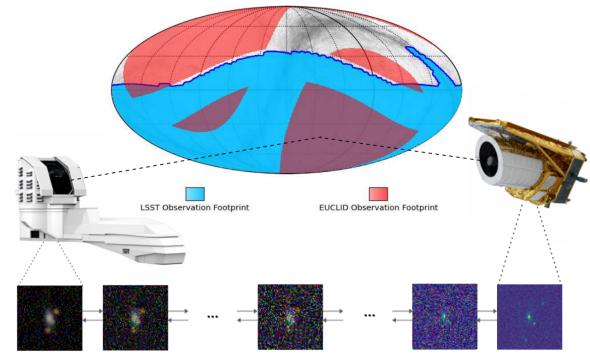


Figure 1: Overview of AS-Bridge. The central panel shows the visible sky, with the LSST and Euclid survey footprints marked in blue and red, respectively. The overlapping regions indicate areas jointly observed by the ground-based LSST (left) and the space-based Euclid mission (right). LSST provides multi-band optical images that are more blended due to atmospheric seeing, while Euclid delivers sharper near-infrared observations from space. From these overlapping regions, matched image cutouts are extracted and used to train AS-Bridge, which models the probabilistic translation between the two survey domains using a Brownian bridge formulation.

Fundamental differences in observational modality—such as Point Spread Functions (PSFs), noise statistics, photometric band-passes, and scanning cadence—introduce systematic distribution shifts that complicate cross-survey inference.

The mapping between ground-based and space-based imaging is inherently ill-posed in both directions. Recovering Euclid-quality morphology from LSST requires resolving ambiguity induced by atmospheric blurring and background noise. Conversely, mapping Euclid observations back to the LSST domain requires inferring spectral information from fewer and different bands, making the relationship non-identifiable from a single deterministic mapping. Therefore, inter-survey translation should be treated as a probabilistic process that can sample multiple valid realizations consistent with the available observations.

To model this probabilistic process, we introduce AS-Bridge, a unified bidirectional generative framework designed to model the

stochastic connection between survey domains. AS-Bridge formulates inter-survey translation as a bidirectional Brownian bridge process, learning a stochastic path that connects the LSST and Euclid data distributions using overlapping sky regions as anchors. This formulation explicitly models the probabilistic transition between the two surveys and enables calibrated probabilistic inference in both directions.

We demonstrate the following benefits from inter-survey generation:

Inter-survey restoration and synthesis. After training on paired cutouts—currently from simulations, but which can be readily constructed once official data releases become available after camera calibration—AS-Bridge can generate complementary observations in non-overlapping sky regions. We show that AS-Bridge recovers the target-survey observation conditioned on the source-survey input, and empirically demonstrate superior probabilistic reconstruction quality compared to competing baselines (Sec. 4.3.2). This enables analyses developed for one survey to be transferred to regions observed only by the other, while preserving uncertainty quantification.

Inter-survey rare event detection. We cast rare-event detection as inter-survey inconsistency under uncertainty. At inference time, a paired observation is mapped into the inter-survey bridge and reconstructed back to one domain; the reconstruction inconsistency, aggregated over multiple stochastic samples, serves as an anomaly score. This yields an anomaly detector that simultaneously exploits complementary observational modalities through cross-survey conditioning and probabilistic reconstruction along the diffusion bridge. We demonstrate improved detection of strong gravitational lenses as a representative example of structural outliers, compared to general-purpose baselines.

Our contributions are as follows:

- We introduce the inter-survey modeling problem and formulate probabilistic inter-survey inference for next-generation cosmological surveys by treating cross-survey translation as an ill-posed, bidirectional inference problem. We further identify rare event detection as a key downstream application enabled by this formulation.
- We propose AS-Bridge, a generative framework that models inter-survey translation as a bidirectional Brownian bridge process, recovers the target conditional distribution given the source survey observation, and enables rare event detection through inter-survey probabilistic inconsistency.
- We construct the first realistic simulated benchmark for this problem and systematically compare AS-Bridge against representative baseline methods under standardized evaluation protocols and metrics.

2 Background and Related Work

2.1 Next-Generation Astronomical Surveys

This decade marks a paradigm shift in observational cosmology driven by the emergence of wide-field, high-throughput sky surveys. These next-generation surveys aim to map the Universe with unprecedented depth, angular resolution, spectral coverage, and temporal cadence, enabling precision studies of cosmology, galaxy evolution, and time-domain phenomena at scale.

Among them, the ground-based Legacy Survey of Space and Time (LSST) [19] at the Vera C. Rubin Observatory, the space-based Euclid mission, the Nancy Grace Roman Observatory [26], the Square Kilometer Array (SKA) [1] and the Simon’s Observatory. In this paper we focus on LSST and Euclid, as these are the first surveys on the sky with high complementary in resolution and temporal cadence.

LSST is a deep, multi-band optical imaging survey conducted by the Vera C. Rubin Observatory, located on Cerro Pachón in northern Chile. Its southern-hemisphere location enables continuous access to a large, contiguous region of the southern sky. Over a planned ten-year survey, LSST will repeatedly image approximately $18,000 \text{ deg}^2$ of sky across six optical bands (u, g, r, i, z, y), with a typical revisit cadence of a few days. The telescope features an effective aperture of 6.7 m and a 9.6 deg^2 field of view, producing images with a typical seeing-limited angular resolution of ~ 0.7 arcsec.

The strengths of LSST lie in its exceptional depth, temporal coverage, and statistical power, making it particularly well suited for studies of large-scale structure, weak gravitational lensing, and transient and variable phenomena. However, as a ground-based survey, LSST observations are affected by atmospheric turbulence, variable seeing conditions, sky background, and weather-dependent systematics.

In contrast, Euclid [10] is a space-based mission operated by the European Space Agency, designed to deliver high-resolution imaging and near-infrared photometry and spectroscopy over a wide area of the extragalactic sky. Free from atmospheric effects, Euclid provides stable and sharply defined point-spread functions, enabling precise galaxy shape measurements. Euclid carries two primary instruments: the VIS instrument, which provides high-resolution optical imaging in a broad visible band with a pixel scale of 0.1 arcsec, and the NISP instrument, which performs near-infrared imaging and slitless spectroscopy across the $Y, J,$ and H bands.

Euclid is expected to survey approximately $15,000 \text{ deg}^2$ of the extragalactic sky, avoiding regions of high Galactic extinction and stellar density. Its primary science objectives focus on probing dark energy and dark matter through weak gravitational lensing and galaxy clustering, leveraging high-fidelity shape measurements and well-controlled instrumental systematics. However, compared to LSST, Euclid operates with fewer photometric bands and a different observational cadence, and its near-infrared focus results in complementary—but incomplete—spectral information relative to ground-based optical surveys.

The survey footprints of LSST and Euclid overlap significantly, with an estimated common area of $\sim 7,000\text{--}9,000 \text{ deg}^2$, depending on final survey strategies and masking. In these overlapping regions, both surveys observe the same underlying astrophysical objects but produce fundamentally different data realizations due to differences in angular resolution, wavelength coverage, noise statistics, and survey strategy. To date, most strong-lensing searches have been conducted within single-survey data sets, with training sets and detection pipelines tailored to the characteristics of that specific survey. These systematic differences induce non-trivial distribution shifts between the two datasets. As a result, direct joint analysis is challenging: models and measurements developed for one survey cannot be naively transferred to the other, and simple deterministic

mappings fail to capture the intrinsic ambiguities and uncertainties between observational modalities.

2.2 Strong Gravitational Lensing

Strong gravitational lensing occurs when a massive foreground galaxy (the deflector) lies close to the line of sight to a more distant background source, bending the source light strongly enough to produce multiple images and high-magnification features. For extended background galaxies, this typically appears as multiple arcs or a nearly complete Einstein ring. If the background galaxy also hosts a compact point source—such as an AGN, quasar, or supernova—the lens can additionally produce multiple point-like images, commonly observed as “doubles” (two images) or “quads” (four images). Systems dominated by extended lensed galaxies are often referred to as galaxy–galaxy lenses, while those highlighted by multiply imaged point sources are described using the double/quad terminology.

Compared to ordinary galaxy detections, strong lenses are much rarer because they require a special combination of conditions—most importantly, a near alignment between the foreground deflector and the background source. As a result, only a small fraction of galaxies on the sky exhibit recognizable strong-lensing morphologies in survey images.

In this work, we treat strong gravitational lenses as representative rare events. Although their physical nature is well understood, we intentionally treat them as unknown anomalies at test time, and evaluate whether the model can detect them purely through inter-survey probabilistic inconsistency.

2.3 Image Translation

Image-to-Image (I2I) translation studies how to transform an image from a *source* visual domain \mathcal{X} to a *target* visual domain \mathcal{Y} . Given $x \in \mathcal{X}$, the goal is to synthesize $y \in \mathcal{Y}$ that retains the underlying semantics (e.g., geometry, layout, identity) but adopts domain-specific appearance statistics (e.g., texture, color distribution, sensor characteristics).

Early practical I2I systems were largely driven by GANs, including pix2pix [18], SPADE [27], and OASIS [30]. More recently, diffusion models have emerged as a leading framework for image-to-image translation due to their stable training dynamics and likelihood-based generative formulation. Denoising Diffusion Probabilistic Models (DDPMs) [14] define a forward process that gradually perturbs data with Gaussian noise and learn the corresponding reverse denoising dynamics for sampling. Conditional diffusion extends this framework to translation tasks by conditioning the reverse process on a source image, achieving strong performance across a wide range of I2I applications. Palette [29] provides a unified conditional diffusion framework for multiple restoration-style I2I problems.

In conditional diffusion pipelines such as Palette, target images are generated by reversing a diffusion process initialized from pure Gaussian noise, while the source image is incorporated solely as an external conditioning signal. An alternative formulation is provided by bridge-based diffusion models, which directly model a stochastic transition between two domain distributions. Brownian Bridge [23, 25] defines a forward process between source and target

domains, rather than between data and pure noise. This formulation leads to more efficient sampling by avoiding unnecessary diffusion through high-noise states. In our work, we show that training Brownian bridges with an appropriate weighting term not only yields high-quality reconstructions but also fits better to the underlying conditional distribution.

Finally, although GAN-based, diffusion-based, and bridge-based methods can all generate multiple outputs for a single input, they are typically developed and evaluated under a single-direction point-estimation paradigm and evaluated on deterministic metrics. In contrast, scientific applications require models that faithfully represent the full conditional distribution between observational modalities. This motivates our focus on probabilistic inter-domain modeling and bidirectional inference beyond conventional I2I evaluation protocols.

2.4 Anomaly Detection

One of the high-impact opportunities of next-generation surveys is the discovery of “unknown unknowns”—rare astrophysical events that challenge current astrophysical or cosmological models. This task can be characterized as Anomaly Detection (AD). Current approaches in astrophysics predominantly focus on temporal anomalies (transients) [7, 8, 13, 17]. The standard pipeline involves extracting light-curve features followed by classical outlier detection algorithms like Isolation Forests [24]. While effective for time-domain events, these methods struggle to identify structural static anomalies—such as galaxy-galaxy strong gravitational lenses and other unique morphological irregularities—which require structural semantic understanding rather than temporal feature extraction.

Industrial visual anomaly detection (e.g., defect inspection) has recently converged on diffusion-based reconstruction [3, 11]: a diffusion model is trained on normal data and anomalies are detected via elevated reconstruction/denoising error in regions that deviate from in-distribution examples. Similar reconstruction-based diffusion paradigms have also shown promise in medical imaging settings [35].

More recently, multimodal anomaly detection benchmarks have been proposed to integrate complementary sensory inputs, such as combining 2D images with 3D point clouds [6, 34]. These methods typically rely on explicit feature fusion modules to aggregate modality-specific representations and define anomaly scores based on cross-modal discrepancy.

3 Method

3.1 Survey Translation Formulation

Let the intrinsic light omission process underlying an astronomical object be denoted by Φ . In practice, this process is not observed directly. Instead, observations are produced through the telescope and detector via a sequence of survey-specific operations, including convolution with the point-spread function (PSF), spectral integration over a limited set of wavelength bands determined by the instrument filters, and the addition of stochastic noise sources.

We model the observation process of a given survey as

$$x = O(\Phi) + \epsilon(O(\Phi)), \quad (1)$$

where \mathcal{O} denotes the deterministic observation operator incorporating PSF convolution and bandpass integration, and $\epsilon(\cdot)$ represents signal-dependent noise, including photon noise as well as signal-independent components such as readout and instrumental noise.

We consider two astronomical surveys observing the same underlying astrophysical scene but with different instrumental and observational characteristics. Rather than treating one survey as a source domain and the other as a target domain, we view the observations as two distinct realizations of a shared latent astrophysical process, shaped by survey-specific effects such as atmosphere, optics, point-spread functions, noise statistics, and spectral bandpasses. Formally, the two observations can be written as

$$\begin{aligned} x_{\text{Euclid}} &= \mathcal{O}_{\text{Euclid}}(\Phi) + \epsilon_{\text{Euclid}}(\mathcal{O}_{\text{Euclid}}(\Phi)), \\ x_{\text{LSST}} &= \mathcal{O}_{\text{LSST}}(\Phi) + \epsilon_{\text{LSST}}(\mathcal{O}_{\text{LSST}}(\Phi)). \end{aligned} \quad (2)$$

The latent process Φ is fundamentally unobservable: there exists no experiment, even in principle, that provides access to a noiseless, fully resolved, all-band representation of a distant astronomical object. Therefore, we marginalize over the unobserved latent process Φ and focus on learning the relationship between different observational realizations. Since each observation captures only a partial and noisy projection of the underlying scene, neither x_{Euclid} nor x_{LSST} fully determines the other. The mapping between surveys is therefore inherently stochastic rather than deterministic. We model the cross-survey relationship through the conditional distributions $p(x_{\text{Euclid}} | x_{\text{LSST}})$ and $p(x_{\text{LSST}} | x_{\text{Euclid}})$.

Our goal is to learn a single generative framework that jointly captures both conditionals, enabling bidirectional translation between surveys while preserving shared astrophysical structure and explicitly modeling the uncertainty induced by incomplete observations and signal-dependent noise. Under this formulation, given an observation from either survey, the model can sample plausible realizations of how the same object would appear if observed by the other survey.

3.2 AS-Bridge Framework

In this section, we first give a brief introduction to Brownian bridge diffusion and its training objectives used in previous work. We then derive a better training objective that balances between reconstruction fidelity and data likelihood which are equally important for probabilistic reconstruction problems.

3.2.1 Brownian Bridge. A Brownian bridge [37] can be viewed as a Gaussian stochastic process obtained by conditioning Brownian motion on fixed endpoints. In contrast to standard diffusion, which progressively destroys information from a single source, a Brownian bridge performs a stochastic interpolation between two observations.

Given two endpoints (x_0, x_T) , Brownian bridge motion between them is defined as

$$dx_t = \frac{x_0 - x_T}{1 - m_t} dt + dW_t, \quad 0 \leq t < T, \quad (3)$$

where W_t is the standard Brownian motion and $m_t = \frac{t}{T}$. The closed-form solution is

$$x_t = x_0 + m_t(x_T - x_0) + (W_t - m_t W_T). \quad (4)$$

The conditional distribution of x_t given x_0 and x_T is

$$x_t | (x_0, x_T) \sim \mathcal{N}((1 - m_t)x_0 + m_t x_T, \delta_t I), \quad (5)$$

where $\delta_t = m_t(1 - m_t)$.

The reverse transition is obtained from Bayes' theorem [14, 23]:

$$p_\theta(x_{t-1} | x_t, x_1) = \frac{q(x_t | x_{t-1}, x_t) q(x_{t-1} | x_0, x_t)}{q(x_t | x_0, x_T)} = \mathcal{N}(\tilde{\mu}_t, \delta_{t|t-1} I). \quad (6)$$

where

$$\tilde{\mu}_t = a_t x_t + b_t x_T - c_t (m_t(x_T - x_0) + \sqrt{\delta_t} \epsilon), \quad (7)$$

with coefficients

$$a_t = \frac{\delta_{t-1}}{\delta_t} \frac{1 - m_t}{1 - m_{t-1}} + \frac{\delta_{t|t-1}}{\delta_t} (1 - m_t), \quad (8)$$

$$b_t = m_{t-1} - m_t \frac{1 - m_t}{1 - m_{t-1}} \frac{\delta_{t-1}}{\delta_t}, \quad (9)$$

$$c_t = (1 - m_t) \frac{\delta_{t|t-1}}{\delta_t}, \quad (10)$$

and variance schedule

$$\delta_{t|t-1} = \delta_t - \delta_{t-1} \frac{(1 - m_t)^2}{(1 - m_{t-1})^2}. \quad (11)$$

Previous works using Brownian bridge [14, 23] optimize the following loss

$$\mathcal{L} = \mathbb{E}_{x_0, x_T, t, \epsilon} \left[\left\| \left(m_t(x_T - x_0) + \sqrt{\delta_t} \epsilon \right) - f_\theta(x_t, x_T, t) \right\|_2^2 \right]. \quad (12)$$

which is the drift term plus the denoising term in a single timestep.

3.2.2 Maximum Likelihood Training. Song et al. [32] showed that score-based diffusion models can be trained by maximum likelihood through a properly weighted denoising score matching objective. Under variance-exploding (VE) diffusion, the likelihood objective leads to a timestep-dependent weighting proportional to δ_t . While the data is gradually blended so the total variance is preserved in standard DDPM [15], VE diffusion defines the diffusion process where the data variance preserve so the total variance increases as the noise scale δ_t grows. Since the source and target observations are two different realizations of the same underlying astronomical object, we assume that the marginal data variance of the two domains is identical, which matches the VE assumption.

Both Song et al. [32] and Ho et al. [14] observed that introducing this weighting often results in slightly worse FID. However, Song et al. demonstrated that this weighting significantly improves the estimated data likelihood.

For scientific problems involving probabilistic reconstruction, our goal is to ensure that the learned reverse process matches the conditional probability distribution. Therefore, we prefer an objective that better aligns with maximum likelihood as well as perceptual quality.

However, directly using δ_t as the weighting term in Brownian bridge training leads to vanishing weights at both endpoints of the bridge. When optimizing for guaranteed maximum likelihood, such vanishing weights prevent the model from being effectively trained at the endpoints.

To mitigate this issue, we propose to train the Brownian bridge with an ϵ -prediction loss. We formally prove that the ϵ -prediction

loss is equivalent to the standard loss times a milder weight $\sqrt{\delta_t}$, which preserves the likelihood-inspired emphasis on high-noise timesteps while maintaining stable gradients across the bridge. Empirical results in Tab. 1 show that ϵ -prediction yields the best reconstruction performance under uncertainty.

PROPOSITION 1. *Training with ϵ -prediction loss is equivalent to training with the loss define in Eq. (12) with a milder weighting term $\sqrt{\delta_t}$.*

PROOF. From Eq. (5), the forward process satisfies

$$x_t = \mu_t + \sqrt{\delta_t} \epsilon, \quad (13)$$

where $\epsilon \sim \mathcal{N}(0, I)$.

The true score of x_t is

$$\nabla_{x_t} \log p(x_t) = -\frac{x_t - \mu_t}{\delta_t} = -\frac{\epsilon}{\sqrt{\delta_t}}. \quad (14)$$

If the network predicts noise $\epsilon_\theta(x_t, t)$, the implied score estimate is

$$s_\theta(x_t, t) = -\frac{\epsilon_\theta(x_t, t)}{\sqrt{\delta_t}}. \quad (15)$$

Starting from the weighted denoising score matching loss

$$\mathcal{L} = \sqrt{\delta_t} \|s_\theta(x_t, t) - \nabla_{x_t} \log p(x_t)\|_2^2, \quad (16)$$

and substituting the expressions in terms of ϵ , we obtain

$$\mathcal{L} = \sqrt{\delta_t} \left\| -\frac{\epsilon_\theta}{\sqrt{\delta_t}} + \frac{\epsilon}{\sqrt{\delta_t}} \right\|_2^2 = \|\epsilon_\theta - \epsilon\|_2^2. \quad (17)$$

□

With ϵ -prediction, the estimated target at each timestep \hat{x}_0 can be derived based on Eq.(13)

$$\hat{x}_0 = \frac{x_t - m_t x_T - \sqrt{\delta_t} \epsilon_\theta(x_t, x_T, t)}{1 - m_t} \quad (18)$$

3.3 Rare event detection

We leverage the trained inter-survey generative model as an unsupervised anomaly detector. The core assumption is that rare or previously unseen astrophysical phenomena are underrepresented in the training distribution and therefore cannot be faithfully reconstructed by the model.

Given paired observations (x_{Euclid}, x_{LSST}) from two surveys, we generate an intermediate variable x_t by stochastically fusing the two observations according to the Brownian bridge forward process defined in Eq. (5). Starting from this noisy fusion, we progressively apply the learned reverse dynamics to reconstruct the original observations in each survey domain. Since the prediction of LSST observations is more uncertain than the prediction of Euclid, we use only the Euclid reconstruction error as the anomaly score.

Unlike previous reconstruction-based anomaly detection methods that directly compare a single reconstruction with the ground truth, astronomical images typically exhibit low signal-to-noise ratios, causing reconstruction errors to be dominated by mismatches in random noise rather than meaningful structural deviations. To mitigate this issue, we sample multiple reconstructions from the

same noisy fusion. Given N stochastic reconstructions $\{\hat{x}_0^{(i)}\}_{i=1}^N$, we define a pixel-wise anomaly map as

$$\mathcal{A}(p) = \min_{i \in \{1, \dots, N\}} \|\hat{x}_0^{(i)}(p) - x_0(p)\|_2^2, \quad (19)$$

and the image-level anomaly score is obtained by flux-normalized aggregation, avoiding bias toward brighter objects,

$$\mathcal{A}(x_0) = \frac{\sum_p \mathcal{A}(p)}{\sum_p x_0(p)}. \quad (20)$$

By taking the minimum error across multiple stochastic reconstructions, this score suppresses spurious errors caused by noise fluctuations while remaining sensitive to systematic reconstruction failures.

4 Experiments

4.1 Dataset Generation

Euclid data products are becoming publicly available, while Rubin has revealed first imagery and early previews, with LSST science operations approaching but not yet represented by a fully mature public survey stream. To enable a controlled and survey-comparable development setting for cross-survey learning, we construct a forward-modeled dataset of galaxy observations under Euclid (VIS band) and LSST (g, r, i bands) imaging. The dataset is built from astrophysically motivated population synthesis and rendered through survey-specific instrument transfer functions.

Using SLSIM [9], we generate two image sets: regular galaxies and galaxy-galaxy strong-lens systems. Regular galaxies are drawn directly from the simulated galaxy catalogs (after basic selection cuts on, e.g., redshift and magnitude). Galaxy-galaxy lenses are produced by pairing foreground deflectors with background sources from the same catalogs and forward-modeling the resulting lensing configurations, retaining only systems that satisfy our detectability criteria (e.g., sufficient image separation and brightness).

In total, we generate 115,000 regular galaxies and 5,000 galaxy-galaxy strong lenses. We use 110,000 regular galaxies for training, and reserve the remaining regular galaxies together with all lens systems for evaluation and downstream tasks.

4.1.1 Cosmology Configuration. We assuming a flat Λ CDM cosmology with $H_0 = 70 \text{ km s}^{-1} \text{ Mpc}^{-1}$ and $\Omega_m = 0.3$. This fixes the angular-diameter distances that set the lensing geometry and the characteristic angular scale of Einstein radii.

4.1.2 Regular Galaxy Population. We generate mock galaxy catalogs using SkyPy [2] over $z \in [0, 5]$ with $\Delta z = 0.1$ and limiting magnitude $m_{\text{lim}} = 30$ while sampling from an effective sky area of 0.1 deg^2 .

We synthesize two physically interpretable galaxy populations: blue (late-type) and red (early-type) systems.

For each galaxy, we sample its redshift and absolute magnitude from redshift-evolving Schechter luminosity functions, assign a spectral energy distribution using Dirichlet mixtures of kcorrect-style templates, compute stellar mass and apparent magnitudes in Euclid and LSST bands, and draw structural properties (e.g., angular size and ellipticity) from population-dependent statistical priors.

This produces realistic regular galaxies with physically grounded photometry and morphology. We instantiate two catalogs for different purposes: one catalog is used to render the regular galaxy samples for the dataset, while a second catalog is used as the parent population from which deflectors and sources are selected for constructing strong lens systems.

4.1.3 Strong Lens Population. Using the second catalog, we use the SL_{SIM} to construct galaxy–galaxy strong lens systems by explicitly separating *deflectors* and *sources* according to astrophysical priors.

Deflectors: drawn from red and blue populations, filtered with $0.1 < z_d < 2$ and $i < 24$.

Sources: drawn from the blue population, filtered with $0.1 < z_s < 5$ and $i < 26$, and modeled as single Sérsic extended sources.

Lens systems: rendered over a nominal sky area of 10 deg^2 , with image separation $0.8'' < \Delta\theta < 10''$, and a brightness cut applied to the second-brightest lensed image.

This produces a physically realistic distribution of galaxy–galaxy strong lenses consistent with cosmology and galaxy evolution.

4.1.4 Cross-survey Bandpass Harmonization. To ensure photometric consistency across surveys, we harmonize bandpass definitions using `spec1lite` [20]. We adopt Euclid VIS and LSST 2016 bandpasses (`lsst2016-g`, `lsst2016-r`, `lsst2016-i`).¹

4.1.5 Multi-survey Image Rendering (Euclid VIS, LSST g, r, i). Both regular galaxies and lens systems are rendered into 64×64 pixel cutouts using survey-specific instrument models.²

For each object (regular or lens), we render a Euclid VIS image and LSST g, r , and i single-band images.

This produces paired cross-survey observations of the same underlying astrophysical object, observed through distinct instrument transfer functions (PSF, pixel scale, exposure, noise).

4.2 Qualitative Evaluation and Potential Scientific Impact

In this section, we qualitatively show the reconstruction examples of different start and end points of AS-Bridge and discuss how they may benefit downstream scientific analysis.

4.2.1 LSST \rightarrow Euclid. LSST observations are frequently affected by atmospheric seeing and PSF broadening, which cause nearby galaxies to merge into a single apparent source in crowded regions. In contrast, Euclid VIS provides significantly higher spatial resolution from space, clearly separating these systems and revealing their true multi-object structure. Galaxy demographics and weak lensing shape measurements rely critically on accurate measurements of galaxy counts, positions, and morphologies. When blended systems in LSST are misidentified as single objects, systematic biases are introduced into number counts and downstream population statistics. As shown in Fig. 2 inferring from LSST to Euclid, AS-Bridge can separate blended systems and reconstruct a physically consistent

¹Because the Euclid VIS response contains extremely small non-zero values outside its effective wavelength range, which interferes with simulations over $z \in [0, 5]$, we truncate the VIS filter to the official Euclid wavelength range of 5500–9000 Å. This avoids introducing non-physical flux contributions during SED integration.

²To avoid truncating extended lensing features in the lower-resolution LSST images (where the broader PSF and coarser sampling spread the signal over a larger apparent area), we choose the cutout field of view to be sufficiently large for LSST instead of the same FOV of Euclid.

multi-object scene from LSST observations, enabling more reliable demographic analysis on LSST-only sky region.

4.2.2 Euclid \rightarrow LSST. Reconstructing LSST multi-band color information from a single Euclid VIS observation is an extremely ill-posed problem, as Euclid collapses most spectral information into a broad band. However, Euclid still provides strong morphological cues and near-infrared intensity patterns that are statistically correlated with optical color. AS-Bridge learns this implicit conditional relationship between morphology, near-infrared brightness, and multi-band optical appearance across the two surveys.

As shown in Fig. 3, the model consistently preserves the morphological structure across multiple stochastic realizations while producing color variations that remain centered around the ground truth LSST observation. The diversity of these samples reflects the inherent uncertainty of the task, yet the ground truth lies well within the distribution of generated reconstructions. Tab. 1 quantitatively evaluates the quality of this reconstruction. This capability enables the analysis of plausible LSST band information for Euclid-only detections under uncertainty.

4.2.3 LSST \leftrightarrow Euclid. AS-Bridge learns to reconstruct typical in-distribution galaxy morphologies from the noisy fusion of LSST and Euclid observations. As shown in Fig. 1, for common systems such as high-inclination disk galaxies, the model accurately recovers the elongated structure, demonstrating that it successfully captures the dominant galaxy population.

However, for rare galaxy–galaxy strong-lensing systems, the model exhibits a systematic reconstruction failure. This behavior arises because AS-Bridge has implicitly learned the statistical priors of regular galaxies, such as centrally concentrated brightness profiles and smooth curvature patterns. Small deviations from these learned priors—even when barely perceptible to the human eye—can fall outside the learned distribution and lead to incorrect reconstructions.

In Fig. 4, the model reconstructs the arc of a partially observable Einstein ring as a three point-source system. This discrepancy between the true Euclid observation and the AS-Bridge Euclid reconstruction provides a natural signal for anomaly and rare-event detection.

4.3 Quantitative Evaluation

While the qualitative examples above illustrate the potential scientific impact of AS-Bridge, we next formalize this evaluation through quantitative metrics and comparisons with competing methods. These experiments establish a benchmark for future methods developed under our problem formulation and dataset.

4.3.1 Metrics. Evaluating AI models for scientific discovery requires metrics that address domain-specific constraints beyond standard computer vision tasks. First, telescope observation is inherently stochastic; thus, a model must not only minimize error but also correctly quantify observational uncertainty. Second, in the search for rare phenomena, the metric must reflect the practical workflow of domain experts, where the cost of verifying false positives is the limiting factor. Accordingly, we assess our framework

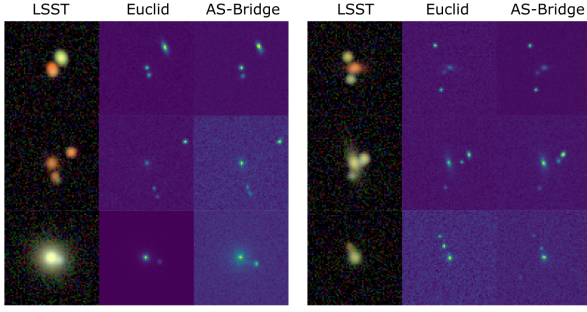


Figure 2: LSST-to-Euclid translation. Left: LSST where nearby galaxies are strongly blended due to atmospheric seeing and PSF broadening. Middle: Euclid observation revealing the true multi-object structure at higher spatial resolution. Right: AS-Bridge reconstruction from the LSST input, correctly recovering the number of galaxies and accurately localizing their centers.

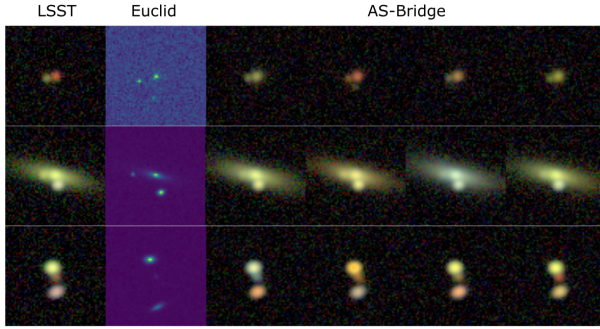


Figure 3: Euclid-to-LSST translation with multiple realizations. From left to right: LSST observation, Euclid observation, and four stochastic LSST reconstructions generated by AS-Bridge from the Euclid input. While Euclid provides high-resolution morphology but limited spectral information, AS-Bridge reconstructs plausible LSST multi-band appearances that preserve the underlying structure and produce color variations consistent with the ground truth.

using two complementary sets of metrics: Probabilistic Reconstruction Quality to validate physical calibration, and Detection Metrics to evaluate discovery efficiency.

To evaluate the probabilistic reconstruction quality of our Brownian Bridge model, we adopt the *Continuous Ranked Probability Score* (CRPS) [12], a strictly proper scoring rule for probabilistic predictions.

Given a ground-truth target $y \in \mathbb{R}^d$ and M samples $\{\hat{y}^{(m)}\}_{m=1}^M$ drawn from the model’s predictive distribution, CRPS is defined as

$$\text{CRPS} = \frac{1}{M} \sum_{m=1}^M \left\| \hat{y}^{(m)} - y \right\|_2 - \frac{1}{2M^2} \sum_{m=1}^M \sum_{m'=1}^M \left\| \hat{y}^{(m)} - \hat{y}^{(m')} \right\|_2. \quad (21)$$

Where M is the total number of samples drawn from the stochastic prediction model and $\hat{y}^{(m)}$ is the m -th sample drawn. The first term measures accuracy with respect to the observed sample,

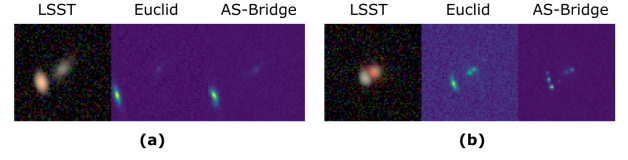


Figure 4: Midpoint-to-Euclid AS-Bridge reconstructions for (a) a system containing a common in-distribution edge-on disk galaxy and (b) a rare galaxy–galaxy strong-lensing system. From left to right: LSST, Euclid, and AS-Bridge reconstruction of Euclid from midpoint. Although the two cases appear visually similar, AS-Bridge faithfully reconstructs the elongated disk morphology in (a), while in (b) it fails to reproduce the extended arc. This facilitates rare event detection.

while the second term penalizes lack of diversity among generated samples, thereby discouraging mode collapse.

CRPS has been widely adopted in scientific prediction tasks that require principled uncertainty quantification, including Weather forecasting [28] and probabilistic segmentation of ambiguous medical images [21].

In the context of astronomical anomaly detection—specifically the identification of rare phenomena in large-scale surveys—the evaluation priorities differ significantly from standard industrial or safety-critical settings.

In industrial defect detection, the goal is typically Recall-oriented (e.g., ensuring no defective part leaves a factory), prioritizing metrics such as the False Positive Rate (FPR) at high True Positive Rates (TPR) (e.g., 95%). However, searching for rare scientific objects in massive datasets is Precision-oriented. The primary constraint is the limited “time budget” of domain experts who must verify candidates. A model that achieves high recall but floods the user with false positives is practically unusable in this domain.

To reflect this “Needle-in-a-Haystack” workflow, we adopt a set of discovery-focused metrics:

- **FPR@lowTPR:** While industrial anomaly detection benchmarks often report the false positive rate (FPR) at 95% true positive rate (TPR), such operating points are impractical for scientific discovery, where recovering nearly all anomalies would require scientists to sift through an overwhelming number of false positives. Instead, we report the FPR at 1% and 5% TPR. This metric measures the fraction of regular objects that scientists would need to inspect in order to recover 1% or 5% of the true anomalies, reflecting a realistic early-discovery regime where verification effort must remain minimal.
- **Area Under the Precision-Recall Curve (AUPR):** Given the extreme class imbalance inherent to astronomical surveys, the standard AUROC can be misleadingly optimistic due to the massive number of True Negatives. We prioritize AUPR, which focuses exclusively on the positive class and penalizes false positives heavily, providing a more robust measure of global detection performance.

4.3.2 *Competing Methods and Results.* For the inter-survey translation task, we compare AS-Bridge of different training objectives

with several other representative generative image translation methods. SPADE [27] is a spatially-adaptive normalization framework that injects semantic layout information into the generator. OASIS [30] is an adversarial semantic image synthesis method that replaces the discriminator with a segmentation network to stabilize training. pix2pix [18] is a conditional GAN for paired image-to-image translation. Palette [29] is a conditional diffusion model that uses the reference image as an additional conditioning signal.

In addition to these baselines, we train a *joint diffusion* model that learns the joint distribution of (x_0, x_T) . During sampling, the observed component is obtained by directly adding noise to the observation according to the forward diffusion process, while the unobserved component is reconstructed through the learned reverse denoising dynamics. This joint-diffusion reconstruction strategy has been widely adopted in scientific inverse problems, including PDE modeling under sparse observations [16] and atlas-based medical image segmentation [36].

Table 1 shows CRPS of AS-Bridge in both directions compared to the aforementioned competing methods. The results show that AS-Bridge with ϵ -prediction objectives achieves the best probabilistic reconstruction performance in both directions. Moreover, diffusion-based and bridge-based methods consistently outperform non-diffusion approaches, highlighting the advantage of score-based generative modeling in recovering the true underlying conditional distributions.

For the anomaly detection task, we compare AS-Bridge with state-of-the-art single-modal and multi-modal industrial anomaly detection methods, namely Deco-Diff [3] and Crossmodal Feature Mapping (CFM) [6].

CFM is originally designed for cross-modal learning between 2D images and 3D point clouds using separate modality-specific encoders. In our setting, we adapt CFM by employing two image encoders to process LSST and Euclid observations respectively.

Table 2 reports the performance of the three rare-event detectors. Deco-Diff, as a single-modal method, fails to identify these events. In contrast, both AS-Bridge and CFM achieve strong performance, highlighting the importance of incorporating multi-sensor information for astronomical rare-event detection. Furthermore, AS-Bridge outperforms CFM. This improvement is likely due to AS-Bridge’s stochastic reconstruction mechanism.

5 Limitations and Ethical Considerations

This work is currently trained and evaluated only on simulated data, and a simulation-to-reality domain gap is expected when transferring the model to real LSST and Euclid observations. It should therefore be regarded as a proof-of-concept. Demonstrating effectiveness in a controlled simulation setting allows us to justify and propose subsequent training on real survey data once they become available, rather than applying the method directly to raw observations without prior validation. This simulation-first validation is a common and well-established practice in astronomy.

This work involves only astronomical data and publicly available survey specifications. No human subjects, personal data, or sensitive information are involved. We do not identify any direct ethical risks associated with this research.

Table 1: Quantitative comparison of Continuous Ranking Probability Score (CRPS) (\downarrow) on bidirectional translation tasks. Lower is better. The best results are highlighted in bold.

Method	CRPS (\downarrow)	
	LSST \rightarrow Euclid	Euclid \rightarrow LSST
<i>Non-diffusion Baselines</i>		
SPADE[20]	3.39	16.52
OASIS[30]	4.65	13.33
Pix2Pix[18]	4.35	73.03
<i>Diffusion Baselines</i>		
Palette[29]	2.43	7.98
Joint	3.14	15.15
<i>AS-Bridge w/ different training objectives</i>		
$m_t(x_T - x_0) + \sqrt{\delta_t}\epsilon$	2.55	7.90
$\sqrt{\delta_t}\epsilon$	3.59	11.24
ϵ	2.38	7.90

Table 2: Quantitative comparison of rare event detection performance. We report FPR@TPR (\downarrow) and Area Under Precision-Recall (AUPR \uparrow). The best results are highlighted in bold.

Method	FPR@1% TPR \downarrow	FPR@5% TPR \downarrow	AUPR \uparrow
AS-Bridge	0.00%	0.18%	0.80
Deco-Diff [3]	1.1%	5.0%	0.61
CFM [6]	0.24%	1.2%	0.75

6 Conclusion

We formulate a probabilistic inter-survey translation problem between the two flagship astronomical surveys, LSST and Euclid, and propose AS-Bridge to model this stochastic relationship. We demonstrate several potential scientific impacts enabled by different choices of bridge start and end points, including deblending merged sources in crowded fields, synthesizing plausible multi-band color information with uncertainty, and detecting rare astronomical events. We expect additional scientific applications of this inter-survey bridge to emerge as the community explores its capabilities.

We further propose task-specific evaluation metrics and compare AS-Bridge against representative competing baselines. Together with the simulated dataset, this work establishes a benchmark for LSST–Euclid translation that can be used for future methodological development and evaluation.

As future work, we plan to deploy this framework on real observations once the official data releases from both surveys become available. We envision an iterative scientific pipeline built around the two core capabilities of AS-Bridge. A base AS-Bridge model, trained on the regular population, serves as a general-purpose translator and a tool for discovering rare events. These rare events, once inspected and categorized by scientists, can then be used to fine-tune category-specific AS-Bridge models, enabling more accurate reconstruction and analysis of objects belonging to particular rare-event classes.

References

- [1] Peter Ade, James Aguirre, Zeeshan Ahmed, Simone Aiola, Aamir Ali, David Alonso, Marcelo A. Alvarez, Kam Arnold, Peter Ashton, Jason Austermann, Humna Awan, Carlo Baccigalupi, Taylor Baildon, Darcy Barron, Nick Battaglia, Richard Battye, Eric Baxter, Andrew Bazarko, James A. Beall, Rachel Bean, Dominic Beck, Shawn Beckman, Benjamin Beringue, Federico Bianchini, Steven Boada, David Boettger, J. Richard Bond, Julian Borrill, Michael L. Brown, Sarah Marie Bruno, Sean Bryan, Erminia Calabrese, Victoria Calafut, Paolo Calisse, Julien Carron, Anthony Challinor, Grace Chesmore, Yuji Chinone, Jens Chluba, Hsiao-Mei Sherry Cho, Steve Choi, Gabriele Coppi, Nicholas F. Cothard, Kevin Coughlin, Devin Crichton, Kevin D. Crowley, Kevin T. Crowley, Ari Cukierman, John M. D'Ewart, Rolando Dünner, Tijmen de Haan, Mark Devlin, Simon Dicker, Joy Didier, Matt Dobbs, Bradley Dober, Cody J. Duell, Shannon Duff, Adri Duivenvoorden, Jo Dunkley, John Dusatko, Josquin Errard, Giulio Fabian, Stephen Feeney, Simone Ferraro, Pedro Fluxà, Katherine Freese, Josef C. Frisch, Andrei Frolov, George Fuller, Brittany Fuzia, Nicholas Galitzki, Patrio A. Gallardo, Jose Tomas Galvez Gherzi, Jiansong Gao, Eric Gawiser, Martina Gerbino, Vera Gluscevic, Neil Goeckner-Wald, Joseph Golec, Sam Gordon, Megan Gralla, Daniel Green, Arpi Grigorian, John Groh, Chris Groppi, Yilun Guan, Jon E. Gudmundsson, Dongwon Han, Peter Hargrave, Masaya Hasegawa, Matthew Hasselfield, Makoto Hattori, Victor Haynes, Masashi Hazumi, Yizhou He, Erin Healy, Shawn W. Henderson, Carlos Hervias-Caimapo, Charles A. Hill, J. Colin Hill, Gene Hilton, Matt Hilton, Adam D. Hincks, Gary Hinshaw, Renée Hložek, Shirley Ho, Shuay-Pwu Patty Ho, Logan Howe, Zhiqi Huang, Johannes Hubmayr, Kevin Hufnberger, John P. Hughes, Anna Ijjas, Margaret Ilike, Kent Irwin, Andrew H. Jaffe, Bhuvnesh Jain, Oliver Jeong, Daisuke Kaneko, Ethan D. Karpel, Nobuhiko Katayama, Brian Keating, Sarah S. Kernasovskiy, Reijo Keski-talo, Theodore Kisner, Kenji Kiuchi, Jeff Klein, Kenda Knowles, Brian Koopman, Arthur Kosowsky, Nicoletta Krachmalnicoff, Stephen E. Kuenstner, Chao-Lin Kuo, Akito Kusaka, Jacob Lashner, Adrian Lee, Eunseong Lee, David Leon, Jason S.-Y. Leung, Antony Lewis, Yaqiong Li, Zack Li, Michele Limon, Eric Linder, Carlos Lopez-Caraballo, Thibaut Louis, Lindsay Lowry, Marius Lungu, Mathew Madhavacheril, Daisy Mak, Felipe Maldonado, Hamdi Mani, Ben Mates, Frederick Matsuda, Loïc Maurin, Phil Mautskopf, Andrew May, Nialh McCallum, Chris McKenney, Jeff McMahon, P. Daniel Meerburg, Joel Meyers, Amber Miller, Mark Mirmelstein, Kavilan Moodley, Moritz Munchmeyer, Charles Munson, Sigurd Naess, Federico Nati, Martin Navaroli, Laura Newburgh, Ho Nam Nguyen, Michael Niemack, Haruki Nishino, John Orlowski-Scherer, Lyman Page, Bruce Partridge, Julien Peloton, Francesca Perrotta, Lucio Piccirillo, Giampaolo Pisano, Davide Poletti, Roberto Puddu, Giuseppe Puglisi, Chris Raum, Christian L. Reichardt, Mathieu Remazeilles, Yoel Rephaeli, Dominik Riechers, Felipe Rojas, Anirban Roy, Sharon Sadeh, Yuki Sakurai, Maria Salatino, Mayuri Sathyanarayana Rao, Emmanuel Schaan, Marcel Schmittfull, Neelima Sehgal, Joseph Seibert, Uros Seljak, Blake Sherwin, Meir Shimon, Carlos Sierra, Jonathan Sievers, Precious Sikhosana, Maximiliano Silva-Feaver, Sara M. Simon, Adrian Sinclair, Praween Sirtanasak, Kendrick Smith, Stephen R. Smith, David Spergel, Suzanne T. Staggs, George Stein, Jason R. Stevens, Radek Stompor, Aritoki Suzuki, Osamu Tajima, Satoru Takakura, Grant Teply, Daniel B. Thomas, Ben Thorne, Robert Thornton, Hy Trac, Calvin Tsai, Carole Tucker, Joel Ullom, Sunny Vagnozzi, Alexander van Engelen, Jeff Van Lanen, Daniel D. Van Winkle, Eve M. Vavagiakis, Clara Vergès, Michael Visser, Kasey Wagoner, Samantha Walker, Jon Ward, Ben Westbrook, Nathan Whitehorn, Jason Williams, Joel Williams, Edward J. Wollack, Zhilei Xu, Byeonghee Yu, Cyndia Yu, Fernando Zago, Hezi Zhang, Ningfeng Zhu, and The Simons Observatory collaboration. 2019. The Simons Observatory: science goals and forecasts. *Journal of Cosmology and Astroparticle Physics* 2019, 02 (feb 2019), 056.
- [2] Adam Amara, Lucia F. de la Bella, Simon Birrer, Sarah Bridle, Juan Pablo Cordero, Ginevra Favole, Ian Harrison, Ian W. Harry, William G. Hartley, Coleman Krawczyk, Andrew Lundgren, Brian Nord, Laura K. Nuttall, Richard P. Rollins, Philipp Sudek, Sut-Ieng Tam, Nicolas Tessore, Arthur E. Tolley, Keiichi Umetsu, Andrew R. Williamson, and Laura Wolz. 2021. 'SkyPy': A package for modelling the Universe. *Journal of Open Source Software* 6, 65 (2021), 3056. doi:10.21105/joss.03056
- [3] Farzad Bezaee, Gregory A Lodygensky, Christian Desrosiers, and Jose Dolz. 2025. Correcting deviations from normality: A reformulated diffusion model for multi-class unsupervised anomaly detection. In *Proceedings of the Computer Vision and Pattern Recognition Conference*. 19088–19097.
- [4] A. Blanchard, S. Camera, C. Carbone, V. F. Cardone, S. Casas, S. Clesse, S. Ilić, M. Kilbinger, T. Kitching, M. Kunz, F. Lacasa, E. Linder, E. Majerotto, K. Marković, M. Martinelli, V. Pettorino, A. Pourtsidou, Z. Sakr, A. G. Sánchez, D. Sapone, I. Tutusaus, S. Yahia-Cherif, V. Yankelevich, S. Andreon, H. Aussel, A. Balaguera-Antolínez, M. Baldi, S. Bardelli, R. Bender, A. Biviano, D. Bonino, A. Boucaud, E. Bozzo, E. Branchini, S. Brau-Nogue, M. Brescia, J. Brinckmann, C. Burigana, R. Cabanac, V. Capobianco, A. Cappi, J. Carretero, C. S. Carvalho, R. Casas, F. J. Castander, M. Castellano, S. Cavuoti, A. Cimatti, R. Cledassou, C. Colodro-Conde, G. Congedo, C. J. Conselice, L. Conversi, Y. Copin, L. Corcione, J. Coupon, H. M. Courtois, M. Cropper, A. Da Silva, S. de la Torre, D. Di Ferdinando, F. Dubath, F. Ducret, C. A. J. Duncan, X. Dupac, S. Dusini, G. Fabbian, M. Fabricius, S. Farrens, P. Fosalba, S. Fotopoulou, N. Fourmanoit, M. Frailis, E. Franceschi, P. Franzetti, M. Fumana, S. Galeotta, W. Gillard, B. Gillis, C. Giocoli, P. Gómez-Alvarez, J. Graciá-Carpio, F. Grupp, L. Guzzo, H. Hoekstra, F. Hormuth, H. Israel, K. Jahnke, E. Keihanen, S. Kermiche, C. C. Kirkpatrick, R. Kohley, B. Kubik, H. Kurki-Suonio, S. Ligori, P. B. Lilje, I. Lloro, D. Maino, E. Maiorano, O. Marggraf, N. Martinet, F. Marulli, R. Massey, E. Medinaceli, S. Mei, Y. Mellier, B. Metcalf, J. J. Metge, G. Meylan, M. Moresco, L. Moscardini, E. Munari, R. C. Nichol, S. Niemi, A. A. Nucita, C. Padilla, S. Paltani, F. Pasian, W. J. Percival, S. Pires, G. Polenta, M. Poncet, L. Pozzetti, G. D. Racca, F. Raison, A. Renzi, J. Rhodes, E. Romelli, M. Roncarelli, E. Rossetti, R. Saglia, P. Schneider, V. Scottez, A. Secroun, G. Sirri, L. Stanco, J.-L. Starck, F. Sureau, P. Tallada-Crespí, D. Tavagnacco, A. N. Taylor, M. Tenti, I. Tereno, R. Toledo-Moreo, F. Torradeflot, L. Valenziano, T. Vassallo, G. A. Verdoes Kleijn, M. Viel, Y. Wang, A. Zacchei, J. Zoubian, and E. Zucca. 2020. Euclid preparation: VII. Forecast validation for Euclid cosmological probes. *Astronomy & Astrophysics* 642 (Oct. 2020), A191. doi:10.1051/0004-6361/202038071
- [5] The LSST Dark Energy Science Collaboration, Rachel Mandelbaum, Tim Eifler, Renée Hložek, Thomas Collett, Eric Gawiser, Daniel Scolnic, David Alonso, Humna Awan, Rahul Biswas, Jonathan Blazek, Patricia Burchat, Nora Elisa Chisari, Ian Dell'Antonio, Seth Digel, Josh Frieman, Daniel A. Goldstein, Isobel Hook, Željko Ivezić, Steven M. Kahn, Sowmya Kamath, David Kirkby, Thomas Kitching, Elisabeth Krause, Pierre-François Leget, Philip J. Marshall, Joshua Meyers, Hiromao Miyatake, Jeffrey A. Newman, Robert Nichol, Eli Rykoff, F. Javier Sanchez, Anže Slosar, Mark Sullivan, and M. A. Troxel. 2021. The LSST Dark Energy Science Collaboration (DESC) Science Requirements Document. arXiv:1809.01669 [astro-ph.CO] (2021). <https://arxiv.org/abs/1809.01669>
- [6] Alex Costanzino, Pierluigi Zama Ramirez, Giuseppe Lisanti, and Luigi Di Stefano. 2024. Multimodal Industrial Anomaly Detection by Crossmodal Feature Mapping. In *Proceedings of the IEEE Conference on Computer Vision and Pattern Recognition*. CVPR.
- [7] Miguel Crispim Romão, Djuna Croon, and Daniel Godines. 2025. Anomaly detection to identify transients in LSST time series data. *Monthly Notices of the Royal Astronomical Society* 543, 1 (09 2025), 351–357. arXiv:https://academic.oup.com/mnras/article-pdf/543/1/351/64222460/staf1477.pdf doi:10.1093/mnras/staf1477
- [8] N. De Bonis, S. Vaccaro, Y. Maruccia, G. Riccio, R. Crupi, S. Rubini, D. De Cicco, M. Brescia, and S. Cavuoti. 2026. Hunting the outliers: Machine learning for anomalous time series detection. *Astronomy and Computing* 55 (2026), 101049. doi:10.1016/j.ascom.2025.101049
- [9] Khadka et al. and DESC & SLSC Collaboration. 2025. SLSim: Strong Lensing Simulation pipeline. GitHub repository. <https://github.com/LSST-strong-lensing/slsim> Documentation: <https://slsim.readthedocs.io>. Accessed: 2026-01-29.
- [10] Euclid Collaboration, Y. Mellier, Abdurro'uf, J. A. Acevedo Barroso, A. Achúcarro, J. Adamek, R. Adam, G. E. Addison, N. Aghanim, M. Agüena, V. Ajani, Y. Akrami, A. Al-Bahlawan, A. Alavi, I. S. Albuquerque, G. Alestas, G. Alguero, A. Allaoui, S. W. Allen, V. Allevaro, A. V. Alonso-Tetilla, B. Altieri, A. Alvarez-Candal, S. Alvi, A. Amara, L. Amendola, J. Amiaux, I. T. Andika, S. Andreon, A. Andrews, G. Angora, R. E. Angulo, F. Annibali, A. Anselmi, S. Anselmi, S. Arcari, M. Archidiacono, G. Aricò, M. Arnaud, S. Arnouts, M. Asgari, J. Asorey, L. Atayde, H. Atek, F. Atrio-Barandela, M. Aubert, E. Aubourg, T. Auphan, N. Auricchio, B. Aussen, H. Aussel, P. P. Avelino, A. Avgoustidis, S. Avila, S. Awan, R. Azzollini, C. Baccigalupi, E. Bachelet, D. Bacon, M. Baes, M. B. Bagley, B. Bahr-Kalus, A. Balaguera-Antolínez, E. Balbinot, M. Balcells, M. Baldi, I. Baldry, A. Balestra, M. Ballardini, O. Ballester, M. Balogh, E. Bañados, R. Barbier, S. Bardelli, M. Baron, T. Barreiro, R. Barrena, J.-C. Barriere, B. J. Barros, A. Barthelemy, N. Bartolo, A. Basset, P. Battaglia, A. J. Battisti, C. M. Baugh, L. Baumont, L. Bazzanini, J.-P. Beaulieu, V. Beckmann, A. N. Belikov, J. Bel, F. Bellagamba, M. Bella, E. Bellini, K. Benabed, R. Bender, G. Benevento, C. L. Bennett, K. Benson, P. Bergamini, J. R. Bermejo-Climent, F. Bernardreau, D. Bertacca, M. Berthe, J. Berthier, M. Bethermin, F. Beutler, C. Bevilton, S. Bhargava, R. Bhatawdekar, D. Bianchi, L. Bisigello, A. Biviano, R. P. Blake, A. Blanchard, J. Blazek, L. Blot, A. Bosco, C. Bodendorf, T. Boenke, H. Böhringer, P. Bolchini, M. Bolzonella, A. Bonchi, M. Bonici, D. Bonino, L. Bonino, C. Bonvin, W. Bon, J. T. Booth, S. Borgani, A. S. Borlaff, E. Borsato, B. Bose, M. T. Botticella, A. Boucaud, F. Bouche, J. S. Boucher, D. Boutigny, T. Bouvard, R. Bouwens, H. Bouy, R. A. A. Bowler, V. Bozza, E. Bozzo, E. Branchini, G. Brando, S. Brau-Nogue, P. Brekke, M. N. Bremer, M. Brescia, M.-A. Breton, J. Brinckmann, T. Brinckmann, C. Brockley-Blatt, M. Brodwin, L. Brouard, M. L. Brown, S. Bruton, J. Bucko, H. Buddelmeijer, G. Buenadicha, F. Buirago, P. Burger, C. Burigana, V. Busillo, D. Busonero, R. Cabanac, L. Cabayol-Garcia, M. S. Cagliari, A. Caillat, L. Caillat, M. Calabrese, A. Calabro, G. Calderone, F. Calura, B. Camacho Quevedo, S. Camera, L. Campos, G. Cañas-Herrera, G. P. Candini, M. Cantiello, V. Capobianco, E. Cappellaro, N. Cappelluti, A. Cappi, K. I. Caputi, C. Cara, C. Carbone, V. F. Cardone, E. Carella, R. G. Carlberg, M. Carle, L. Carminati, F. Caro, J. M. Carrasco, J. Carretero, P. Carrillo, J. Carron Duque, and B. Carry. 2025. Euclid: I. Overview of the Euclid mission. *Astronomy & Astrophysics* 697, Article A1 (May 2025).
- [11] Yaoxuan Feng, Wenchao Chen, Yuxin Li, Bo Chen, Yubiao Wang, Zixuan Zhao, Hongwei Liu, and Mingyuan Zhou. 2025. OmiAD: One-Step Adaptive Masked

- Diffusion Model for Multi-class Anomaly Detection via Adversarial Distillation. In *Proceedings of the 42nd International Conference on Machine Learning (Proceedings of Machine Learning Research, Vol. 267)*, Aarti Singh, Maryam Fazel, Daniel Hsu, Simon Lacoste-Julien, Felix Berkenkamp, Tegan Maharaj, Kiri Wagstaff, and Jerry Zhu (Eds.), PMLR, 16604–16633. <https://proceedings.mlr.press/v267/feng25b.html>
- [12] Tilmann Gneiting and Adrian E Raftery. 2007. Strictly Proper Scoring Rules, Prediction, and Estimation. *J. Amer. Statist. Assoc.* 102, 477 (2007), 359–378.
- [13] Pablo Gómez, Roland D. Vavrek, Guillermo Buenadicha, John Hoar, Sandor Kruk, and Jan Reerink. 2024. Machine learning-driven Anomaly Detection and Forecasting for Euclid Space Telescope Operations. arXiv:2411.05596 [cs.LG] <https://arxiv.org/abs/2411.05596>
- [14] Jonathan Ho, Ajay Jain, and Pieter Abbeel. 2020. Denoising Diffusion Probabilistic Models. *arXiv preprint arxiv:2006.11239* (2020).
- [15] Jonathan Ho, Ajay Jain, and Pieter Abbeel. 2020. Denoising Diffusion Probabilistic Models. *arXiv preprint arxiv:2006.11239* (2020).
- [16] Jiahe Huang, Guandao Yang, Zichen Wang, and Jeong Joon Park. 2024. DiffusionPDE: Generative PDE-Solving Under Partial Observation. arXiv:2406.17763 [cs.LG]
- [17] E. E. O. Ishida, M. V. Kornilov, K. L. Malanchev, M. V. Pruzhinskaya, A. A. Volnova, V. S. Korolev, F. Mondon, S. Sreejith, A. A. Malancheva, and S. Das. 2021. Active anomaly detection for time-domain discoveries. *Astronomy & Astrophysics* 650 (June 2021), A195. doi:10.1051/0004-6361/202037709
- [18] Phillip Isola, Jun-Yan Zhu, Tinghui Zhou, and Alexei A Efros. 2017. Image-to-Image Translation with Conditional Adversarial Networks. *CVPR* (2017).
- [19] Željko Ivezić, Steven M. Kahn, J. Anthony Tyson, Bob Abel, Emily Acosta, Robyn Allsman, David Alonso, Yusra AlSayyad, Scott F. Anderson, John Andrew, James Roger P. Angel, George Z. Angeli, Reza Ansari, Pierre Antilogus, Constanza Araujo, Robert Armstrong, Kirk T. Arndt, Pierre Astier, Éric Aubourg, Nicole Auza, Tim S. Axelrod, Deborah J. Bard, Jeff D. Barr, Aurelian Barrau, James G. Bartlett, Amanda E. Bauer, Brian J. Bauman, Sylvain Baumont, Ellen Bechtol, Keith Bechtol, Andrew C. Becker, Jacek Becla, Cristina Beldica, Steve Bellavia, Federica B. Bianco, Rahul Biswas, Guillaume Blanc, Jonathan Blazek, Roger D. Blandford, Josh S. Bloom, Joanne Bogart, Tim W. Bond, Michael T. Booth, Anders W. Borgland, Kirk Borne, James F. Bosch, Dominique Boutigny, Craig A. Brackett, Andrew Bradshaw, William Nielsen Brandt, Michael E. Brown, James S. Bullock, Patricia Burchat, David L. Burke, Gianpiero Cagnoli, Daniel Calabrese, Shawn Callahan, Alice L. Callen, Jeffrey L. Carlin, Erin L. Carlson, Srinivasan Chandrasekharan, Glenaver Charles-Emerson, Steve Chesley, Elliott C. Cheu, Hsin-Fang Chiang, James Chiang, Carol Chirion, Derek Chow, David R. Ciardi, Charles F. Claver, Johann Cohen-Tanugi, Joseph J. Cockrum, Rebecca Coles, Andrew J. Connolly, Kem H. Cook, Asantha Cooray, Kevin R. Covey, Chris Cribbs, Wei Cui, Roc Cutri, Philip N. Daly, Scott F. Daniel, Felipe Daruich, Guillaume Daubard, Greg Daues, William Dawson, Francisco Delgado, Alfred Dellapenna, Robert de Peyster, Miguel de Val-Borro, Seth W. Digel, Peter Doherty, Richard Dubois, Gregory P. Dubois-Felsmann, Josef Durech, Frossie Economou, Tim Eifler, Michael Eracleous, Benjamin L. Emmons, Angelo Fausti Neto, Henry Ferguson, Enrique Figueroa, Merlin Fisher-Levine, Warren Focke, Michael D. Foss, James Frank, Michael D. Freeman, Emmanuel Gangler, Eric Gawiser, John C. Geary, Perry Gee, Marla Geha, Charles J. B. Gessner, Robert R. Gibson, D. Kirk Gilmore, Thomas Glanzman, William Glick, Tatiana Goldina, Daniel A. Goldstein, Iain Goodenow, Melissa L. Graham, William J. Gressler, Philippe Gris, Leanne P. Guy, Augustin Guyonnet, Gunther Haller, Ron Harris, Patrick A. Hascall, Justine Haupt, Fabio Hernandez, Sven Herrmann, Edward Hileman, Joshua Hoblitt, John A. Hodgson, Craig Hogan, James D. Howard, Dajun Huang, Michael E. Huffer, Patrick Ingraham, Walter R. Innes, Suzanne H. Jacoby, Bhuvnesh Jain, Fabrice Jammes, M. James Jee, Tim Jenness, Garrett Jernigan, Darko Jevremović, Kenneth Johns, Anthony S. Johnson, Margaret W. G. Johnson, R. Lynne Jones, Claire Juramy-Gilles, Mario Jurić, Jason S. Kalirai, Nitya J. Kallivayalil, Bryce Kalmbach, Jeffrey P. Kantor, Pierre Karst, Mansi M. Kasliwal, Heather Kelly, Richard Kessler, Veronica Kinnison, David Kirkby, Lloyd Knox, Ivan V. Kotov, Victor L. Krabbendam, K. Simon Krughoff, Petr Kubánek, John Kuczewski, Shri Kulkarni, John Ku, Nadine R. Kurita, Craig S. Lage, Ron Lambert, Travis Lange, J. Brian Langton, Laurent Le Guillou, Deborah Levine, Ming Liang, Kian-Tat Lim, Chris J. Lintott, Kevin E. Long, Margaux Lopez, Paul J. Lotz, Robert H. Lupton, Nate B. Lust, Lauren A. MacArthur, Ashish Mahabal, Rachel Mandelbaum, Thomas W. Markiewicz, Darren S. Marsh, Philip J. Marshall, Stuart Marshall, Morgan May, Robert McKeercher, Michelle McQueen, Joshua Meyers, Myriam Migliore, Michelle Miller, and David J. Mills. 2019. LSST: From Science Drivers to Reference Design and Anticipated Data Products. *The Astrophysical Journal* 873, 2, Article 111 (March 2019), 111 pages.
- [20] David Kirkby et al. 2024. *desihub/speclite: Bug fix release: General clean-up prior to refactoring package infrastructure (v0.20)*. doi:10.5281/zenodo.13225530
- [21] Simon A. A. Kohl, Bernardino Romera-Paredes, Clemens Meyer, Jeffrey De Fauw, Joseph R. Ledsam, Klaus H. Maier-Hein, S. M. Ali Eslami, Danilo Jimenez Rezende, and Olaf Ronneberger. 2018. A Probabilistic U-Net for Segmentation of Ambiguous Images. In *Advances in Neural Information Processing Systems 31 (NeurIPS 2018)*.
- [22] Jacob A. Kurlander, Pedro H. Bernardinelli, Megan E. Schwamb, Mario Jurić, Joseph Murtagh, Colin Orion Chandler, Stephanie R. Merritt, David Nesvorný, David Vokrouhlický, R. Lynne Jones, Grigori Fedorets, Samuel Cornwall, Matthew J. Holman, Siegfried Eggl, Drew Oldag, Maxine West, Jeremy Kubica, Peter Yoachim, Joachim Moeyens, Kathleen Kiker, and Laura E. Buchanan. 2025. Predictions of the LSST Solar System Yield: Near-Earth Objects, Main Belt Asteroids, Jupiter Trojans, and Trans-Neptunian Objects. *The Astronomical Journal* 170, 2 (July 2025), 99. doi:10.3847/1538-3881/add685
- [23] Bo Li, Kaitao Xue, Bin Liu, and Yu-Kun Lai. 2023. BBDM: Image-to-image translation with Brownian bridge diffusion models. In *Proceedings of the IEEE/CVF Conference on Computer Vision and Pattern Recognition*. 1952–1961.
- [24] Fei Tony Liu, Kai Ming Ting, and Zhi-Hua Zhou. 2008. Isolation Forest. In *2008 Eighth IEEE International Conference on Data Mining*. 413–422. doi:10.1109/ICDM.2008.17
- [25] Zonglin Lyu, Ming Li, Jianbo Jiao, and Chen Chen. 2024. Frame Interpolation with Consecutive Brownian Bridge Diffusion. In *Proceedings of the 32nd ACM International Conference on Multimedia (MM '24)*.
- [26] Gregory Mosby, Bernard J. Rauscher, Chris Bennett, Edward S. Cheng, Stephanie Cheung, Analia Cillis, David Content, Dave Cottingham, Roger Foltz, John Gygas, Robert J. Hill, Jeffrey W. Kruk, Jon Mah, Lane Meier, Chris Merchant, Laddawan Mikko, Eric C. Piquette, Augustyn Wacziarg, and Yiting Wen. 2020. Properties and characteristics of the Nancy Grace Roman Space Telescope H4RG-10 detectors. *Journal of Astronomical Telescopes, Instruments, and Systems* 6, Article 046001 (Oct. 2020), 046001 pages.
- [27] Taesung Park, Ming-Yu Liu, Ting-Chun Wang, and Jun-Yan Zhu. 2019. Semantic Image Synthesis with Spatially-Adaptive Normalization. In *Proceedings of the IEEE Conference on Computer Vision and Pattern Recognition*.
- [28] Stephan Rasp, Stephan Hoyer, Alexander Merose, Ian Langmore, Peter Battaglia, Tyler Russel, Alvaro Sanchez-Gonzalez, Vivian Yang, Rob Carver, Shreya Agrawal, Matthew Chantry, Zied Ben Bouallegue, Peter Dueben, Carla Bromberg, Jared Sisk, Luke Barrington, Aaron Bell, and Fei Sha. 2023. WeatherBench 2: A benchmark for the next generation of data-driven global weather models. arXiv:2308.15560 [physics.ao-ph]
- [29] Chitwan Saharia, William Chan, Huiwen Chang, Chris Lee, Jonathan Ho, Tim Salimans, David Fleet, and Mohammad Norouzi. 2022. Palette: Image-to-image diffusion models. In *ACM SIGGRAPH 2022 conference proceedings*. 1–10.
- [30] Edgar Schonfeld, Vadim Sushko, Dan Zhang, Juergen Gall, Bernt Schiele, and Anna Khoreva. 2021. You Only Need Adversarial Supervision for Semantic Image Synthesis. In *International Conference on Learning Representations*. <https://openreview.net/forum?id=yvQKLqN6M>
- [31] Megan E. Schwamb, R. Lynne Jones, Steven R. Chesley, Alan Fitzsimmons, Wesley C. Fraser, Matthew J. Holman, Henry Hsieh, Darin Ragozzine, Cristina A. Thomas, David E. Trilling, Michael E. Brown, Michele T. Bannister, Dennis Bode-wits, Miguel de Val-Borro, David Gerdes, Mikael Granvik, Michael S. P. Kelley, Matthew M. Knight, Robert L. Seaman, Quan-Zhi Ye, and Leslie A. Young. 2018. Large Synoptic Survey Telescope Solar System Science Roadmap. *arXiv e-prints*, Article arXiv:1802.01783 (Feb. 2018), arXiv:1802.01783 pages.
- [32] Yang Song, Conor Durkan, Iain Murray, and Stefano Ermon. 2021. Maximum Likelihood Training of Score-Based Diffusion Models. In *Thirty-Fifth Conference on Neural Information Processing Systems*.
- [33] Tom Wagg, Mario Juric, Peter Yoachim, Jake Kurlander, Sam Cornwall, Joachim Moeyens, Siegfried Eggl, R. Lynne Jones, and Peter Birtwhistle. 2025. Expected Impact of Rubin Observatory LSST on NEO Follow-up. *The Astronomical Journal* 169, 6 (may 2025), 315. doi:10.3847/1538-3881/adc89f
- [34] Yue Wang, Jinlong Peng, Jiangning Zhang, Ran Yi, Yabiao Wang, and Chengjie Wang. 2023. Multimodal Industrial Anomaly Detection via Hybrid Fusion. In *Proceedings of the IEEE/CVF Conference on Computer Vision and Pattern Recognition*. 8032–8041.
- [35] Julia Wolleb, Florentin Bieder, Robin Sandkühler, and Philippe C. Cattin. 2022. Diffusion Models for Medical Anomaly Detection. In *Medical Image Computing and Computer Assisted Intervention – MICCAI 2022*, Linwei Wang, Qi Dou, P. Thomas Fletcher, Stefanie Speidel, and Shuo Li (Eds.). Springer Nature Switzerland, Cham, 35–45.
- [36] Hantao Zhang, Yuhe Liu, Jiancheng Yang, Weidong Guo, Xinyuan Wang, and Pascal Fua. 2025. DiffAtlas: GenAI-fying Atlas Segmentation via Image-Mask Diffusion. In *proceedings of Medical Image Computing and Computer Assisted Intervention – MICCAI 2025*, Vol. LNCS 15975. Springer Nature Switzerland.
- [37] Bernt Øksendal. 2003. *Stochastic Differential Equations: An Introduction with Applications*. Springer.